IEEE Robotics and Automation Letters (RA-L) paper, presented at ICRA 2026, Vienna, Austria. Cite as RA-L paper.

Biarticular Rigid Powered Lower Extremity Exoskeleton Robot

Tianchi Chen[1], Zhi Liu[1], Chaoyang Li[2], Xiaoan Chen[1], Jianjun Hu[1], Jiaxun Wu[1] and Ye He[1]

***Abstract*—Lower extremity exoskeletons designed for multi-joint assistance are increasingly explored for rehabilitation and human augmentation. However, conventional monoarticular designs often suffer from joint misalignment and actuator redundancy, limiting their efficiency and user comfort. This study presents a biarticular rigid powered lower extremity exoskeleton that simultaneously assists the knee and ankle joints through a single actuator, enabling coordinated torque generation across adjacent joints. A hierarchical control framework combining gait segmentation, impedance-based torque generation, and gravity/friction compensation is implemented to provide phase-specific assistance. Experimental results show that the proposed exoskeleton reduces gastrocnemius activation by up to 63.4% and metabolic cost by up to 11.6% during stair ascent, with corresponding reductions of 28.3% and 8.2% during level walking. These findings demonstrate the effectiveness of the biarticular and underactuated structure in enhancing locomotor efficiency, highlighting its potential as a compact and practical solution for dynamic and diverse mobility scenarios.**

***Index Terms*—Prosthetics and Exoskeletons, Biologically-Inspired Robots, Hardware-Software Integration in Robotics.**

I. Introduction

Wearable robotic exoskeletons have shown significant promise in applications ranging from rehabilitation and mobility assistance to human performance augmentation. Among them, lower limb exoskeletons have garnered particular attention due to their direct impact on walking and daily locomotion. With ongoing advances in mechanical design and control strategies, many systems have demonstrated the ability to reduce the metabolic cost of locomotion under various conditions [1-5].

Early exoskeleton designs often employed rigid monoarticular configurations, wherein each joint was actuated independently by a dedicated motor. This approach simplified mechanical layout and control design [6-10]. However, mounting multiple actuators along the limb, especially distally, introduces substantial additional mass, which disrupts natural gait dynamics, increases metabolic energy expenditure, and elevates physical burden on the wearer. Moreover, independently actuated joints lack intrinsic coordination, requiring sophisticated synchronization strategies to avoid unnatural joint behaviors and inefficient energy transfer [11].

A further challenge lies in the complex anatomical structure of human joints. Contrary to simplified assumptions, joint rotation axes do not lie purely within the sagittal plane but span across three-dimensional space [12]. This makes it difficult for monoarticular actuators to maintain precise alignment with human joint centers, especially under dynamic conditions. Misalignment can result in suboptimal torque delivery, reduced comfort, and compromised biomechanical efficiency [13]. Additionally, not all joints require high-torque assistance simultaneously during gait. Assigning separate actuators to each joint leads to functional redundancy, unnecessary system complexity, and elevated energy consumption.

To address these limitations, recent research has explored biarticular exoskeletons, which employ a single actuator to simultaneously assist two adjacent joints. This approach aims to improve both energy transfer efficiency and joint coordination. Simulation studies have shown that biarticular configurations are less sensitive to inertial penalties and can achieve comparable or even superior metabolic benefits with lower actuator torque requirements compared to monoarticular designs [14].

Experimental investigations further support the advantages of biarticular architectures. By mimicking muscle-tendon paths that span two joints (typically the hip and knee or the knee and ankle), various biarticular systems have been developed using cable-driven mechanisms or compliant elements [15-18]. For instance, the multi-joint system developed by Lee et al.[19] reduced the metabolic cost of loaded walking by more than 14%, significantly outperforming comparable monoarticular devices. Similarly, Malcolm et al. [15] reported that their biarticular configuration using pneumatic artificial muscles reduced metabolic energy expenditure by approximately 13%, nearly twice the improvement achieved by comparable monoarticular systems. Beyond energy efficiency, biarticular structures have also been shown to preserve more natural joint kinematics and gait patterns, thereby minimizing disruption to users' habitual motor behaviors.

Despite these advantages, many biarticular exoskeletons are implemented in soft or quasi-passive forms, which come with their own limitations [20-24]. For example, the Myosuit [25] employs textile-based structures and cable transmissions to provide hip and knee extension assistance. It

This work was supported by the National Science and Technology Major Project of the Ministry of Science and Technology of China under Grant 2024ZD0714801, the Ministry of Science and Technology High-end Foreign Experts Recruitment Plan of China under Grant G2022165013L, and the Graduate Scientific Research and Innovation Foundation of Chongqing, China under Grant CYB19062. *(Corresponding author: Ye He.)*

This work involved human subjects or animals in its research. Approval of all ethical and experimental procedures and protocols was granted by Chongqing University Cancer Hospital Ethics Committee under Application No. CZLS2021070-A.

[1]T. C., Z. L., X.C., J. H., J. W., and Y. H. are with the State Key Laboratory of Mechanical Transmission for Advanced Equipment and the College of Mechanical and Vehicle Engineering, Chongqing University, 400044, Chongqing, China. (e-mail: chentcme@foxmail.com; liuzhierd@hotmail.com; xachen@cqu.edu.cn; hujianjun@cqu.edu.cn; 202407021278T@stu.cqu.edu.cn; h1166@cqu.edu.cn).

[2]C. L. is with College of Intelligent Engineering, Chongqing City Management College, 401331, Chongqing, China. (e-mail: lizhaoyang@cqc.edu.cn).

IEEE Robotics and Automation Letters (RA-L) paper, presented at ICRA 2026, Vienna, Austria. Cite as RA-L paper.

has been shown to reduce electromyographic activity of the extensor muscles during stair ascent [26]. However, these systems often rely on elastic components or low-output actuators, which limit their overall assistance capacity and make precise control more challenging. Other systems like BATEX exoskeleton [27] use series elastic actuators and hybrid control modes to emulate muscle-like behavior, improving compliance and adaptability, but still fall short of the high support torque and structural robustness that rigid exoskeletons can provide.

Passive biarticular mechanisms have also been explored [17, 28]. For instance, Van Dijk et al. [29] proposed a passive elastic tendon that spans the knee and ankle joints, allowing energy storage and return during gait. Although simulation results suggested potential reductions in joint mechanical work, human trials showed only minor reductions in metabolic energy expenditure [30, 31]. These outcomes indicate that purely passive methods may be limited in their ability to provide effective assistance, due to added mass and lack of adaptive control.

By contrast, rigid exoskeletons offer distinct advantages in delivering high torque output and precise control. However, most rigid exoskeletons reported to date remain limited to monoarticular designs, and the integration of biarticular structures within rigid systems has yet to be fully explored. Incorporating biarticular architectures into rigid exoskeletons could combine the benefits of biomechanical coordination and structural robustness, offering a promising path to improving overall system performance and user experience.

In response to these challenges, this study proposes a biarticular rigid powered lower extremity exoskeleton robot (BRPLEE) that integrates a shared mechanical transmission to simultaneously assist the knee and ankle joints. By coordinating actuation across two joints using a rigid linkage, the system aims to retain high output capability while more effectively reducing muscular activation and metabolic energy cost. The proposed design is experimentally validated in typical activities to demonstrate its feasibility and effectiveness.

II. BRPLEE System Modeling

A. Design Requirements

To ensure that the BRPLEE effectively balances biomechanical assistance, structural compactness, and user comfort, several design requirements were explicitly defined at the outset. These requirements guided the mechanical and control implementation and are summarized in Table I.

Based on these requirements, the final BRPLEE mechanical implementation was realized, as detailed in the following subsection.

B. Mechanical Structure

The BRPLEE consists of an adjustable anthropomorphic frame with two custom-designed actuator modules, each mounted on the user's thigh and heel. Each module incorporates a frameless high-torque micro-DC motor (RE40, Maxon, Switzerland), a 2:1 toothed belt, and a ball screw mechanism driven by an incremental encoder (HEDL 5540, AVAGO, USA), providing up to 200 mm of linear extension. The system weighs approximately 8 kg and accommodates users ranging from 165 to 185 cm in height and up to 120 kg in total load (including body weight and carried payload). The knee and ankle joints are actively actuated in the sagittal plane through a biarticular linkage, while the hip joint remains entirely passive. As shown in Figure 1, the exoskeleton is secured to the pelvic, thigh, and foot segments via adjustable straps and medical-grade pads, which help distribute interface pressure and minimize skin irritation. Four custom length adjusters enable user-specific fitting and ensure compatibility with natural lower-limb movement during both walking and stair ascent.

TABLE I. Adopted Design Requirements of BRPLEE

Parameter	Requirement / Value	Notes
Total mass	~8 kg	Includes actuators, structure, and sensors
User height range	165–185 cm	Adjustable frame ensures compatibility
Maximum supported load	⩽120 kg	Includes user body weight and payload
Actuation type	Biarticular rigid linkage	Single actuator assists both knee and ankle joints
Motor torque requirement	Sufficient to reduce GAS activity by >60%	Experimentally validated in stair ascent
Maximum linear extension	200 mm	Provided by ball-screw mechanism
Speed responsiveness	Adequate for treadmill walking (1–3 km/h) and stair ascent	Tested with 5 participants
Compactness & fitting	Adjustable straps, medical pads	To ensure comfort and minimize interface pressure

The measurement system includes inertial measurement units (IMUs), pressure sensors, and surface electromyogram (sEMG) sensors. Among them, the IMUs (JY61P, Witmotion, China) and plantar pressure sensors (RX-D4046, Crownto, China) are embedded components of the exoskeleton system and play a crucial role in its control architecture. IMUs are mounted on the torso, thighs, calves, and feet to estimate joint angles in real time. Specifically, each IMU outputs orientation data in quaternion format at 200 Hz, which is converted into rotation matrices onboard the STM32 microcontroller. The joint angles are then derived by comparing the relative orientations between adjacent limb segments and extracting the sagittal-plane pitch angle via standard Euler decomposition (ZYX convention). Furthermore, since the estimation process relies primarily on inertial data rather than magnetometer readings, and the IMUs are positioned away from the motor drivers, the system remains robust against magnetic disturbances.

The plantar pressure sensors are embedded in the insoles beneath the metatarsal head I (M1) and talus regions. These sensors sample at 100 Hz and are used to identify key gait events such as heel-strike and toe-off. The pressure signals are preprocessed using a 4th-order Butterworth low-pass filter with a cutoff frequency of 10 Hz to reduce noise and improve event detection reliability. The filtered data feed into a finite state machine for gait phase recognition, forming the basis for phase-based assistance control. In contrast, the sEMG sensors (Muscle Electrical Sensor Kit, Sichiray, China) are not part of

IEEE Robotics and Automation Letters (RA-L) paper, presented at ICRA 2026, Vienna, Austria. Cite as RA-L paper.

the control system but are used solely for experimental evaluation. The sEMG signals are collected at 1000 Hz via a wireless amplifier system during testing.

The control system includes a microcontroller (STM32H723VGT6, STMicroelectronics, Switzerland) for data processing and algorithm implementation, a low-power MCU for sensor signal relay (ESP32C3, Espressif Systems, China), two drivers for driving motors and relaying encoder signals (RMDS-303+, Robomodule, China), and the CMSIS-DAP debugger (ESP32S3, Espressif Systems, China) for remote programming. All electrical equipment is contained in a control box at the back of the exoskeleton's waist for easy portability.

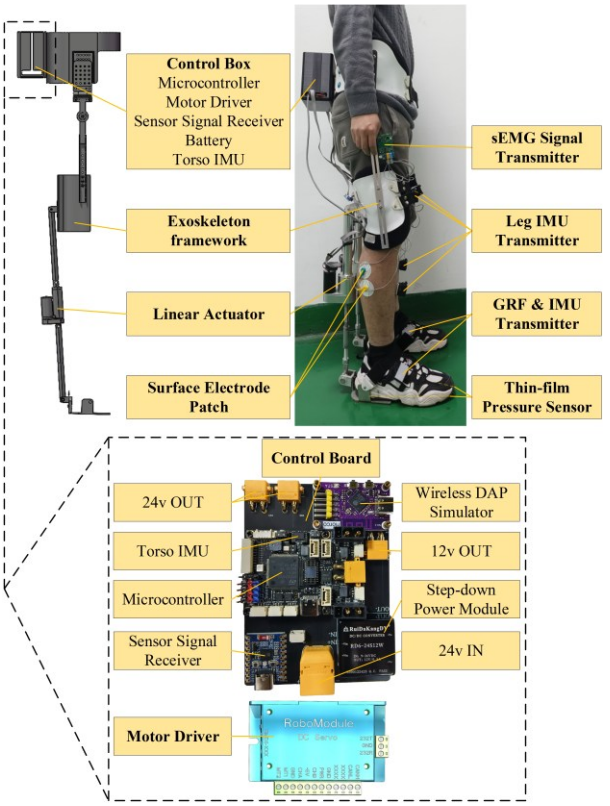

Figure 1. The overall architecture of the BRPLEE.

C. Lower Extremity Biomechanics Model

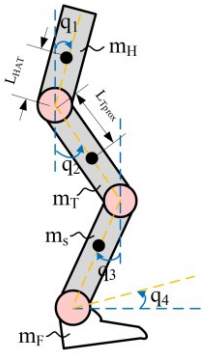

Figure 2. Schematics of the lower extremity biomechanics model.

Figure 2 illustrates a schematic diagram of the biomechanical model of the human lower extremity. The model comprises four segments: the head-arms-trunk (HAT), thigh, shank, and foot, connected by three revolute joints representing the hip, knee, and ankle. The generalized coordinates are marked as $\{q_1,\cdots,q_n\}$. m_H, m_T, m_S, m_F represent the masses of the HAT, thigh, shank, and foot segments. L_{HAT} is the distance from the hip joint to the center of mass of the HAT segment. L_{Thigh} is the distance from the hip joint to the center of mass of the thigh. the mass centers are denoted by black dots. Joint torques $\{\tau_1,\cdots,\tau_n\}$ are applied at the hip, knee, and ankle joints, respectively, and the dynamics are described as:

$$\tau_i=\sum_{j=1}^{n}M_{ij}(q)\ddot{q}_j+\sum_{j=1}^{n}\sum_{k=1}^{n}h_{ijk}(q)\dot{q}_k\dot{q}_j+\sum_{j=1}^{n}m_j\mathbf{g}^T\mathbf{J}_{P_i}^{(j)}(q) \quad (1)$$

where $h_{ijk}=\frac{\partial M_{ij}}{\partial q_k}-\frac{1}{2}\frac{\partial M_{jk}}{\partial q_i}$. $\sum_{j=1}^{n}M_{ij}(q)\ddot{q}_j$ is the inertia term generated by the acceleration of joint; When $k\neq j$, $\sum_{j=1}^{n}\sum_{k=1}^{n}h_{ijk}(q)\dot{q}_k\dot{q}_j$ is the Coriolis force acting on joint i generated by the velocities of joints j and k; $\sum_{j=1}^{n}m_j\mathbf{g}^T\mathbf{J}_{P_i}^{(j)}(q)$ is the gravity term. In the form of matrix and vector, the above formula for joint torque can be rewritten as:

$$\boldsymbol{\tau}=\mathbf{M}(q)\ddot{q}+\mathbf{C}(q,\dot{q})\dot{q}+\mathbf{G}(q) \quad (2)$$

In the human-exoskeleton system,

$$\tau=\tau_{\mathrm{HUMAN}}+\tau_{\mathrm{AC}}+\tau_{\mathrm{H}}-\tau_{\mathrm{EN}}-\tau_{\mathrm{FRICT,EXO}} \quad (3)$$

where τ_{HUMAN} is the active output torque of the joint generated by the human body through muscle activation, τ_{AC} is the driving torque of the exoskeleton joint driver, τ_{H} is the interaction torque between the exoskeleton and the human, τ_{EN} is the reaction torque of the working environment, and $\tau_{\mathrm{FRICT,EXO}}$ is the friction torque of the exoskeleton.

To maximize the assistive effect while ensuring system stability, the value of τ_{HUMAN} should be minimized. Considering that the torques generated by inertial and Coriolis forces are relatively small compared to the gravitational forces during low-speed human movement, and that reducing τ_{HUMAN} to approximately $0\ \mathrm{N\cdot m}$ would increase the error rate in recognizing the human motion intentions within the exoskeleton system, there is also a risk of human losing dominance over the human-exoskeleton system, leading to a significant increase in the probability of instability. Therefore, the proposed control strategy in this study is to appropriately reduce the weight of the inertial and Coriolis forces and use the torque required to counteract gravity as the primary basis for the joint motor output.

III. Gait Analysis and Recognition

A finite state machine (FSM) is utilized to classify gait phases from a control perspective. Seven critical gait events have been identified. Among them, the heel strike event marks

both the initiation of the current gait cycle and the conclusion of the preceding one.

Under normal conditions, gait events progress sequentially as illustrated in Figure 3. The system transitions to the next gait phase only if the current phase is active and the corresponding event is triggered. However, event 7 may transition to event 1 via event 0.

The joint kinematics, including hip, knee, and ankle angles, along with the GRFs at the forefoot and heel, are depicted in Figure 4 for a complete gait cycle. The GRF values have been scaled to the range of 0 to 1 through normalization.

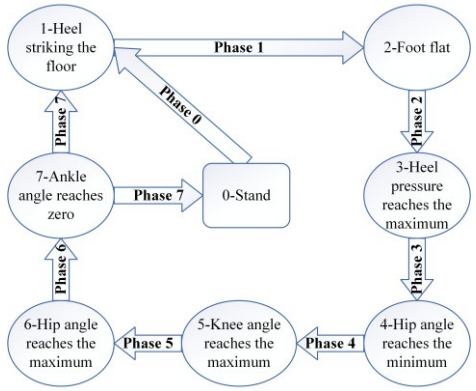

Figure 3. Logic diagram of the FSM.

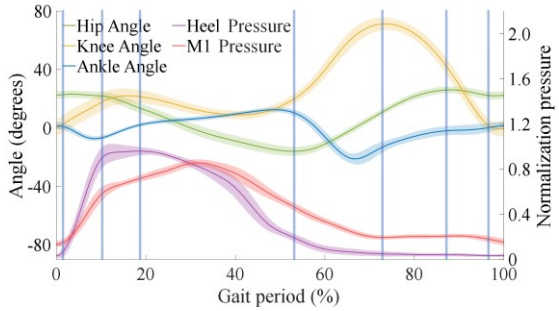

Figure 4. Distribution of gait events over the gait cycle. The left Y-axis is the angle value corresponding to the hip, knee, and ankle curves, and the right Y-axis is the normalized pressure value corresponding to the heel and metatarsal head I curves. The shaded areas indicate the standard deviation of the corresponding curves, and the blue vertical line are gait events.

In contrast to monoarticular exoskeletons, biarticular exoskeletons must consider the effects on multiple joints simultaneously during control. By considering the joint angles and torque requirements of distinct gait phases, we can derive the exoskeleton control states that correspond to each gait phase, as illustrated in Table II.

As shown in Figure 5, this study employs a feedforward neural network (ANN) to train the gait recognition model. The process begins with the normalization of the samples, followed by constructing the target outputs using a one-hot encoding scheme. A two-layer feedforward network is then established: the hidden layer contains 10 neurons with a log-sigmoid activation function, and the output layer consists of 7 neurons with a linear activation function. The model is trained using the gradient descent adaptive learning rate algorithm (traingdx), with appropriate hyperparameters set. Finally, the model's recognition performance is evaluated using the test set. The results, as shown in Figure 6, indicate an accuracy of 96.8%. The misidentifications that occurred were due to small, acceptable errors in gait boundary annotations during the manual data labeling process. These errors do not negatively impact the exoskeleton control strategy following recognition.

TABLE II. DIRECTION OF ASSISTIVE TORQUE AT JOINT IN DIFFERENT GAIT PHASE

Gait Phase	Hip	Knee	Ankle	BRPLEE
0	-	-	-	Follow-up
1	Follow-up	Flexion	Plantarflexion	Follow-up
2	Extension	Flexion	Dorsiflexion	Follow-up
3	Extension	Extension	Dorsiflexion	Extension
4	Flexion	Flexion	Plantarflexion	Retraction
5	Flexion	Extension	Dorsiflexion	Extension
6	Extension	Extension	Dorsiflexion	Extension
7	Follow-up	Follow-up	Follow-up	Follow-up

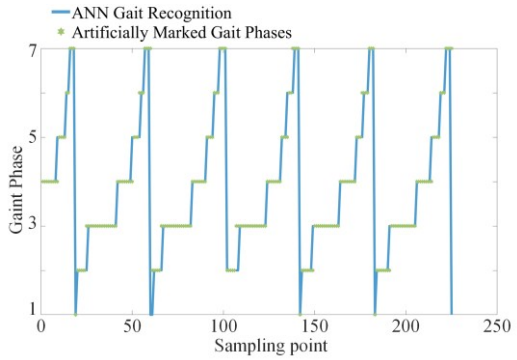

Figure 5. Comparison of ANN-based gait recognition and manual labeling.

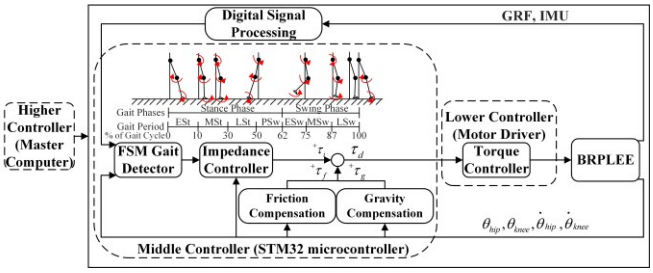

Figure 6. Total control architecture in three different levels.

IV. CONTROL ARCHITECTURE

The control system of BRPLEE is designed based on three-tier architecture, as illustrated in Figure 6. The low-level control employs a proportional–integral–derivative (PID) control algorithm in the motor driver's torque mode to ensure that the output torque τ accurately tracks the desired input torque τ_d The middle-level control module classifies gait phases using a FSM-based gait detector and computes the assistive torques τ_i via an impedance-based control algorithm. Additionally, a model-based feedback friction compensation scheme is implemented to generate the compensated friction torque τ_f, while a gravity compensation scheme produces the gravitational torque τ_g. All algorithms at this level are

IEEE Robotics and Automation Letters (RA-L) paper, presented at ICRA 2026, Vienna, Austria. Cite as RA-L paper.

executed within a microcontroller. The high-level control layer facilitates algorithm development, firmware programming, and remote data monitoring, functioning independently from the exoskeleton during standard operation.

This study employs a model-based feedback friction compensation scheme. As illustrated in Figure 7, the velocity -torque data are acquired through a series of experiments, and the model parameters are identified via curve fitting. The estimated friction torque is then incorporated into the controller through a feedforward mechanism. The friction torque is modeled using the following Stribeck exponential formulation:

$$\boldsymbol{\tau}_f(\omega_m) = \boldsymbol{\tau}_c \cdot sign(\omega_m) + (\boldsymbol{\tau}_s - \boldsymbol{\tau}_c) e^{-(|\omega_m|/\omega_s)^n} + T_v \omega_m \quad (4)$$

The identification and description of the parameters in Equation 4 are shown in Table III.

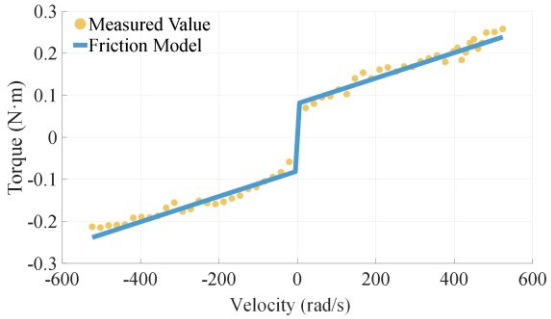

Figure 7. Velocity-torque experimental results and Stribeck model fitting curves.

TABLE III. PARAMETER IDENTIFICATION AND DESCRIPTIONS FOR THE FRICTION COMPENSATION MODEL

Parameter	Value	Description
$\boldsymbol{\tau}_c$	0.0802	Coulomb friction torque
$\boldsymbol{\tau}_s$	0.2000	Static friction torque
ω_s	1.2500	Stribeck velocity
T_v	0.0003	Coefficient of viscous friction
n	3	Exponential parameter

V. EXPERIMENTAL PROTOCOL

Given that the BRPLEE facilitates movement across the knee and ankle joints, mirroring the function of the gastrocnemius (GAS), the reduction in GAS activation was selected as a key metric to evaluate the device's effectiveness. Five healthy adult male participants (age: 23–30 years; height: 176 ± 11 cm; weight: 67.8 ± 6.2 kg) were enrolled. All participants provided informed consent and were free of any orthopedic, muscular, or neurological impairments.

Prior to testing, participants underwent a familiarization phase, during which they practiced walking with the BRPLEE on both a treadmill and stairs. The system initialized the joint angles to zero when the subjects assumed their natural upright posture. Each subject then completed maximal voluntary contraction (MVC) trials by performing ankle plantarflexion sustained for 5 seconds, repeated three times with 3-minute rest intervals to avoid fatigue.

Afterward, participants completed two experimental tasks under both FREE and ASSIST conditions, as illustrated in Figure 8. The first task involved level treadmill walking at three predefined speeds (1 km/h, 2 km/h, and 3 km/h). Each session lasted five minutes, with a mandatory 30-minute rest period between sessions to ensure recovery and mitigate fatigue. The second task focused on stair ascent. For EMG analysis, a custom-built five-step staircase (step height: 17 cm; tread depth: 29 cm) was used, with each trial consisting of three right-legged and two left-legged steps. For metabolic analysis, stair ascent trials were conducted on a standard multi-flight staircase in a real-world environment to ensure sufficient vertical displacement for stable gas exchange measurement. In both tasks, metabolic data were collected using a gas analyzer (MetaLyzer, Cortex Biophysics GmbH, Germany), which recorded breath-by-breath oxygen consumption (VO_2) and carbon dioxide production (VCO_2). Energy expenditure was computed using the Weir equation.

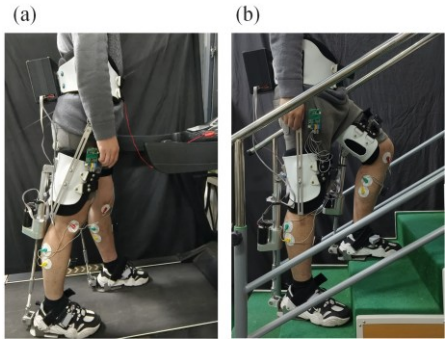

Figure 8. Experimental scenarios of the BRPLEE. (a) Level walking on a treadmill. (b) Stair ascent. The upper limbs are positioned in a manner that reveals the complete extent of the equipment.

Surface EMG signals were recorded at 1000 Hz using a wireless amplifier system and processed offline. Signal processing included band-pass filtering (20–450 Hz), full-wave rectification, and low-pass filtering at 6 Hz to extract the linear envelope. The resulting signals were normalized to peak values obtained from the MVC trials and then averaged to quantify muscle activation levels.

In the FREE mode, participants did not wear the BRPLEE but were equipped with IMUs, plantar pressure sensors, and sEMG sensors to collect baseline data. In the ASSIST mode, the BRPLEE was worn, providing both friction compensation and active gait assistance. IMUs and plantar pressure sensors served as inputs for real-time control, while sEMG sensors monitored muscle activation responses. All data processing and analysis were conducted using MATLAB (R2024b, MathWorks Inc., USA).

VI. RESULTS AND DISCUSSION

As shown in Figure 9, the ASSIST condition significantly reduced GAS activation compared to the FREE condition in both experimental tasks. During level walking, the mean and peak activation intensities decreased by 28.3% and 26.7%, respectively. In stair ascent, the reductions were even more pronounced—55.8% and 63.4%, respectively. These findings indicate that the BRPLEE effectively offloads the GAS

muscle, particularly during more demanding locomotor tasks. Unlike monoarticular systems that focus on a single joint, the BRPLEE provides biarticular assistance, better capturing the functional synergy of biarticular muscles and reducing the user's need to generate compensatory muscle torque.

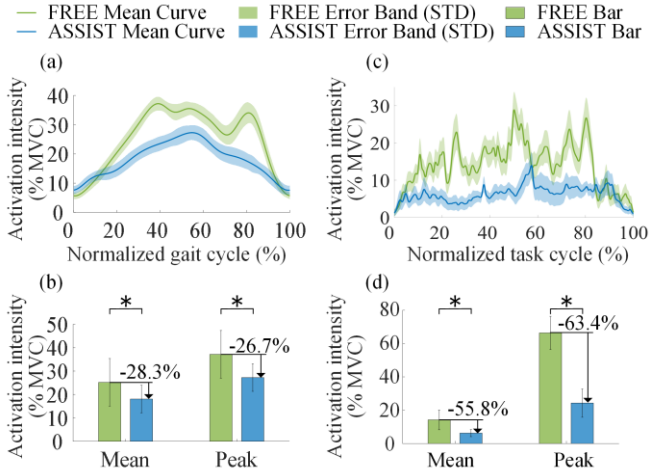

Figure 9. Muscle activation intensity during level walking and stair ascent. (a) and (b) show the comparison between the FREE and ASSIST conditions during level walking, while (c) and (d) correspond to stair ascent. (a) and (c) illustrate the mean normalized muscle activation intensity over a gait or task cycle, respectively. The shaded areas represent the standard deviation of the activation curves. (b) and (d) present the mean and peak activation values within a normalized cycle. Error bars represent standard deviation. The * denotes a significant difference between conditions ($p < 0.05$).

As illustrated in Figure 10, the metabolic cost was also reduced under the ASSIST condition. Specifically, an 8.2% reduction was observed during level walking, and an 11.6% reduction during stair ascent, compared to the FREE condition. The greater benefit observed during stair ascent may be attributed to the increased demand on lower-limb extensors in this task, which is efficiently supported by the biarticular actuation across the knee and ankle joints.

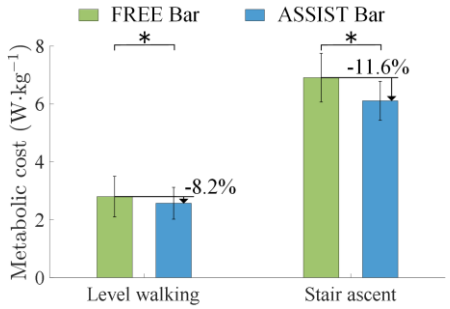

Figure 10. Comparison of metabolic cost between the FREE and ASSIST conditions during level walking and stair ascent. Error bars represent standard deviation. The * indicates a significant difference between the two conditions ($p < 0.05$).

These results are comparable or superior to those reported in previous exoskeleton studies. For instance, Miao et al. proposed a monoarticular rigid hip exoskeleton that achieved a 6.93% metabolic reduction during level walking and 5.75% during stair ascent [32]. Xu et al. developed a soft exosuit assisting hip flexion, which led to a 6.9% reduction in metabolic cost and 9.65% reduction in muscle fatigue during stair ascent [33]. Woo et al. employed a rigid exoskeleton with individual actuators at the hip and knee joints and reported a 9.3% metabolic reduction in stair climbing, though the system weighed 13 kg and was not underactuated [34]. In contrast, the BRPLEE uses a single actuator to power both joints in a structurally compact and energy-efficient manner. Passive designs have also shown moderate effectiveness. Etenzi et al. reported an 11% reduction in walking cost using a passive biarticular knee-ankle device when springs were engaged; however, the system still produced a 23% increase in cost compared to unassisted walking [35]. Galle et al. achieved up to a 12% reduction using a tethered ankle exoskeleton with an external compressed air supply, which eliminated payload on the user but limited system portability [36].

Compared to these approaches, the BRPLEE achieves comparable or superior metabolic reductions while maintaining a fully portable, untethered configuration. Its biarticular, underactuated design enables efficient torque transmission across joints, reducing both the required actuator count and distal mass. This structural simplicity, combined with coordinated assistance during gait, may account for the favorable reductions in energy expenditure observed in both tasks. All reported differences were evaluated using paired t-tests, with statistical significance set at $p < 0.05$.

Although the experimental results are promising, several limitations should be acknowledged. The current study involved a small number of healthy young male participants, limiting generalizability. The assistive torque was conservatively tuned to ensure safety and comfort, suggesting room for further optimization. In addition, all experiments were conducted in controlled laboratory settings. Future work will focus on expanding the participant pool, exploring a broader range of tasks and terrains, and assessing long-term adaptation effects. Further investigation is also warranted into adaptive control strategies for personalized multi-joint assistance.

VII. Conclusion

This paper presents the design, control, and experimental evaluation of BRPLEE—a biarticular, rigid, powered lower-limb exoskeleton that assists both the knee and ankle joints via a single underactuated actuator. The system enables coordinated torque generation across adjacent joints while maintaining a compact and lightweight structure. A hierarchical control framework, comprising a gait segmentation module, an impedance-based torque generator, and compensation for gravity and friction, was implemented to provide task-specific assistance during both level walking and stair ascent.

Experimental results demonstrated that BRPLEE significantly reduced gastrocnemius activation and metabolic cost in both locomotor tasks. Compared to the unassisted condition, muscle activation was reduced by up to 63.4% and net metabolic cost by up to 11.6%. These findings confirm that the biarticular and underactuated design effectively supports multi-joint coordination and improves locomotor efficiency. The integration of mechanical synergy and adaptive control in BRPLEE offers a promising direction for efficient and portable lower-limb assistance. Future work will focus on real-world deployment, user adaptation, and further optimization of assistive profiles to enhance versatility across a broader population and locomotion scenarios.

REFERENCES

[1] Chaoyang Li L L, Zhi Liu, Tianchi Chen, Songxiang Liu, Ye He, Xiaoan Chen, Lei Li, Ang W T. Adaptive control of lower-limb exoskeletons for walking assistance based on inter-joint coordination. Journal of Bionic Engineering. 2024;21(4):1775-1787.

[2] Kalita B, Narayan J, Dwivedy S K. Development of active lower limb robotic-based orthosis and exoskeleton devices: A systematic review. International Journal of Social Robotics. 2021;13(4):775-793.

[3] Martínez-Mata A J, Blanco-Ortega A, Guzmán-Valdivia C H, Abúndez-Pliego A, García-Velarde M A, Magadán-Salazar A, et al. Engineering design strategies for force augmentation exoskeletons: A general review. International Journal of Advanced Robotic Systems. 2023;20(1):17298806221149473.

[4] Grimmer M, Stasica M, Zhao G. Exoskeleton developments at the technical university of darmstadt. in Proceedings of the International Symposium on Technikpsychologie (TecPsy), Darmstadt, Germany; 2023.

[5] Rodríguez-Fernández A, Lobo-Prat J, Font-Llagunes J M. Systematic review on wearable lower-limb exoskeletons for gait training in neuromuscular impairments. Journal of NeuroEngineering and Rehabilitation. 2021;18(1):22.

[6] Lu Z, Ye D, Chen Q, Liu C, Dong H, Cheng D. Adaptive adjustment strategy for walking characteristics of single-legged exoskeleton robots. Machines. 2022;10(2):134.

[7] Nasiri R, Rayati M, Ahmadabadi M N. Feedback from mono-articular muscles is sufficient for exoskeleton torque adaptation. IEEE Transactions on Neural Systems and Rehabilitation Engineering. 2019;27(10):2097-2106.

[8] Song G, Huang R, Qiu J, Cheng H, Fan S. Model-based control with interaction predicting for human-coupled lower exoskeleton systems. Journal of Intelligent & Robotic Systems. 2020;100(2):389-400.

[9] Koda M, Kubota S, Kadone H, Miura K, Funayama T, Takahashi H, et al. Robotic rehabilitation therapy using hybrid assistive limb (hal) for patients with spinal cord lesions: A narrative review. North American Spine Society Journal (NASSJ). 2023;14:100209.

[10] Woods C, Callagher L, Jaffray T. Walk tall: The story of rex bionics. Journal of Management & Organization. 2021;27(2):239-252.

[11] Meng W, Zhu C, Liu H, Liu Q, Xie S. Soft ankle-foot exoskeleton for rehabilitation: A systematic review of actuation, sensing, mechanical design, and control strategy. IEEE Transactions on Medical Robotics and Bionics. 2024;6(2):384-398.

[12] Olinski M, Gronowicz A, Ceccarelli M. Development and characterisation of a controllable adjustable knee joint mechanism. Mechanism and Machine Theory. 2021;155:104101.

[13] Baltrusch S J, Dieen J H v, Bruijn S M, Koopman A S, Bennekom C A M v, Houdijk H. The effect of a passive trunk exoskeleton on metabolic costs during lifting and walking. Ergonomics. 2019;62:903 - 916.

[14] Bonab A K, Patoglu V. Simulation-based multi-criteria comparison of mono-articular and bi-articular exoskeletons during walking with and without load. arXiv preprint arXiv:2110.00062. 2021.

[15] Malcolm P, Galle S, Derave W, De Clercq D. Bi-articular knee-ankle-foot exoskeleton produces higher metabolic cost reduction than weight-matched mono-articular exoskeleton. Frontiers in neuroscience. 2018;12:69.

[16] Schumacher C, Ahmad Sharbafi M, Seyfarth A, Rode C. Biarticular muscles in light of template models, experiments and robotics: A review. Journal of the Royal Society Interface. 2020;17.

[17] Barazesh H, Ahmad Sharbafi M. A biarticular passive exosuit to support balance control can reduce metabolic cost of walking. Bioinspiration & Biomimetics. 2020;15(3):036009.

[18] Chartier C, Elhawary H, Baradaran A, Vorstenbosch J, Xu L, Efanov J I. Tendon: Principles of healing and repair. Seminars in Plastic Surgery. 2021;35:211 - 215.

[19] Lee S, Kim J, Baker L, Long A, Karavas N, Menard N, et al. Autonomous multi-joint soft exosuit with augmentation-power-based control parameter tuning reduces energy cost of loaded walking. Journal of neuroengineering and rehabilitation. 2018;15(1):66.

[20] Di Natali C, Poliero T, Sposito M, Graf E, Bauer C, Pauli C, et al. Design and evaluation of a soft assistive lower limb exoskeleton. Robotica. 2019;37(12):2014-2034.

[21] Babaei Banyarani P, Tarvirdizadeh B, Hadi A. Design and fabrication of a soft wearable robot using a novel pleated fabric pneumatic artificial muscle (pfpam) to assist walking. Sensors and Actuators A: Physical. 2024;370:115278.

[22] Di Natali C, Sadeghi A, Mondini A, Bottenberg E, Hartigan B, De Eyto A, et al. Pneumatic quasi-passive actuation for soft assistive lower limbs exoskeleton. Frontiers in Neurorobotics. 2020;14.

[23] Kim J, Quinlivan B T, Deprey L-A, Arumukhom Revi D, Eckert-Erdheim A, Murphy P, et al. Reducing the energy cost of walking with low assistance levels through optimized hip flexion assistance from a soft exosuit. Scientific Reports. 2022;12(1):11004.

[24] Kim J. *Soft hip exosuit optimization for improving mobility in healthy young adults and individuals with parkinson's disease*. 2022. Harvard University.

[25] Schmidt K, Duarte J E, Grimmer M, Sancho-Puchades A, Wei H, Easthope C S, et al. The myosuit: Bi-articular anti-gravity exosuit that reduces hip extensor activity in sitting transfers. Frontiers in neurorobotics. 2017;11:57.

[26] Kim J, Kim Y, Kang S, Kim S-J. Investigation with able-bodied subjects suggests myosuit may potentially serve as a stair ascent training robot. Scientific Reports. 2023;13(1):14099.

[27] Firouzi V, Davoodi A, Bahrami F, Sharbafi M A. From a biological template model to gait assistance with an exosuit. Bioinspiration & biomimetics. 2021;16(6):066024.

[28] Chang Y, Zhang J, Chen K, Fu C. Design and preliminary evaluation of a clutch-spring lower limb exoskeleton. in 2019 5th International Conference on Control, Automation and Robotics (ICCAR); 2019.

[29] Van Dijk W, Van der Kooij H, Hekman E. A passive exoskeleton with artificial tendons: Design and experimental evaluation. in 2011 IEEE International Conference on Rehabilitation Robotics; 2011: IEEE.

[30] Chen B, Shi C, Zheng C, Zi B, Zhao P, Li Y. Development of lower limb exoskeleton for walking assistance using energy recycled from human knee joint. Journal of Mechanisms and Robotics. 2022;15(5).

[31] Hu B, Liu F, Cheng K, Chen W, Shan X, Yu H. Stiffness optimal modulation of a variable stiffness energy storage hip exoskeleton and experiments on its assistance effect. IEEE Transactions on Neural Systems and Rehabilitation Engineering. 2023;31:1045-1055.

[32] Miao Y, Wang X, Wang S, Li R. Adaptive switching control based on dynamic zero-moment point for versatile hip exoskeleton under hybrid locomotion. IEEE Transactions on Industrial Electronics. 2022;70(11):11443-11452.

[33] Xu Y, Li W, Chen C, Chen S, Wang Z, Yang F, et al. A portable soft exosuit to assist stair climbing with hip flexion. Electronics. 2023;12(11):2467.

[34] Woo H, Kong K, Rha D-w. Lower-limb-assisting robotic exoskeleton reduces energy consumption in healthy young persons during stair climbing. Applied Bionics and Biomechanics. 2021;2021(1):8833461.

[35] Etenzi E, Borzuola R, Grabowski A M. Passive-elastic knee-ankle exoskeleton reduces the metabolic cost of walking. Journal of neuroengineering and rehabilitation. 2020;17(1):104.

[36] Galle S, Malcolm P, Collins S H, De Clercq D. Reducing the metabolic cost of walking with an ankle exoskeleton: Interaction between actuation timing and power. Journal of neuroengineering and rehabilitation. 2017;14(1):35.